

Measuring interactions between tunnel-coupled quantum dots in the quantum Hall regime

C. Livermore,^{a)} D. S. Duncan, and R. M. Westervelt^{b)}

Division of Engineering and Applied Sciences and Department of Physics, Harvard University, Cambridge, Massachusetts 02138

K. D. Maranowski and A. C. Gossard

Materials Department, University of California at Santa Barbara, Santa Barbara, California 93106

(Received 20 November 1998; accepted for publication 25 June 1999)

We present measurements of the relaxation of frustrated charge configurations via tunneling in a double quantum dot in the quantum Hall regime. We studied transport through two quantum dots in series at each of three Landau level filling factors: $\nu=2, 3,$ and 4 . The double dot conductance was measured as a function of the induced charge on each dot and of the interdot tunnel conductance to demonstrate the evolution of the charging diagram with increasing interdot electron tunneling. At all three filling factors, we find that the evolution from well separated to joined dots is complete at an interdot tunnel conductance $G_{\text{int}} \cong e^2/h$, in contrast with the zero magnetic field case. We also observe that the residual interaction energy relative to the charging energy increases above the zero field value. © 1999 American Institute of Physics. [S0021-8979(99)04619-8]

Recent experiments¹⁻⁷ and theories⁸⁻¹⁴ have examined how electron tunneling between quantum dots weakens charge quantization effects on the individual dots. Livermore *et al.*¹ measured zero-bias Coulomb blockade conductance peaks in a series double quantum dot in zero magnetic field. Those measurements mapped out the double dot charging diagram to determine how interdot tunneling relaxes frustrated double dot charge configurations and merges the two dots into one. In zero magnetic field this transition is driven by electron tunneling through two spin channels in the quantum point contact that connects the two dots.⁸⁻¹² When the interdot tunnel conductance $G_{\text{int}} \cong 0$, the two dots are well separated. The dots join into one large, composite dot at $G_{\text{int}} \cong 2e^2/h$.

In this communication we report measurements of interactions between two tunnel-coupled quantum dots in a strong perpendicular field that places the electron gas in the quantum Hall regime. Single dots in the quantum Hall regime have been studied previously.¹⁵⁻²⁷ McEuen *et al.*^{15,16} studied quantum dot addition spectra, and described how the Landau level structure forms compressible and incompressible regions in the quantum dot. Van der Vaart *et al.*^{20,24} and Alphenaar *et al.*^{25,26} studied how a compressible region can form an isolated island within a quantum dot and how the occupation of the island affects transport through the dot as a whole. Such effects are discussed further in Refs. 27 and 28.

In the experiments described here, we use Coulomb blockade transport spectroscopy to measure the double dot charging diagram as a function of magnetic field and the strength of interdot tunneling. In the quantum Hall regime the electron states in the bulk are localized, so transport takes place only through the edge states²⁹ and relaxation of frus-

trated double dot charge configurations is fundamentally different from the zero magnetic field case. Interdot electron tunneling occurs between the outermost Landau level edge state(s) of the two dots, so only one spin channel is involved in interdot electron transport for $0 \leq G_{\text{int}} \leq e^2/h$. Double dot charge relaxation is predicted to be complete at $G_{\text{int}} = e^2/h$ for the case of one spin channel joining the two dots.⁸⁻¹²

Figure 1(a) is a scanning electron micrograph of our device. It consists of two quantum dots defined in series by 10 independently adjustable Cr/Au gates (light regions) on the surface of a GaAs/AlGaAs heterostructure wafer (dark regions) containing a near surface (57 nm) two-dimensional electron gas (2DEG). The 2DEG has a sheet density $n_s \cong 3.4 \times 10^{11} \text{ cm}^{-2}$ and a mobility $\mu \cong 450\,000 \text{ cm}^2/\text{Vs}$. Figure 1(b) is a schematic diagram of the device wiring. By varying the side gate voltage $V_{g1}(V_{g2})$, we can induce charge separately on dot 1 (dot 2). By varying the center point contact voltage V_{q2} , we can independently adjust the interdot conductance G_{int} .

We cooled the device to base temperature (30 mK) in a dilution refrigerator and energized the magnet to an initial field $B=7$ T, placing the electron gas on the quantum Hall plateau to correspond to a Landau level filling factor $\nu=2$. We applied a small ac bias voltage ($5 \mu\text{V}_{\text{rms}}$) across the device and monitored sample conductance with low noise lock-in techniques. The side gate labeled $V_{g1}(V_{g2})$ is coupled to dot 1 (dot 2) by a capacitance $C_{g1} = 45 \pm 4$ aF ($C_{g2} = 43 \pm 4$ aF) as determined from measurements of single dot conductance versus side gate voltage.

We energized all 10 surface gates such that the outer point contacts were in the tunneling regime and the center point contact conductance was in the range $0 \leq G_{\text{int}} \leq e^2/h$. This placed the entire coupled double dot in the Coulomb blockade regime. We then measured conductance through the double dot as a function of the side gate voltages V_{g1} and

^{a)}Present address: Microsystems Technology Laboratories, Room 39-561, Massachusetts Institute of Technology, Cambridge, MA 02139.

^{b)}Electronic mail: westervelt@deas.harvard.edu

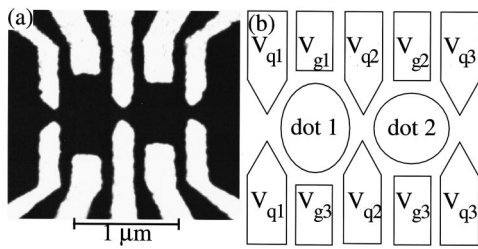


FIG. 1. (a) Scanning electron micrograph of the double quantum dot device. Dark regions are the surface of the GaAs/AlGaAs heterostructure wafer; light regions are the Cr/Au surface gates. (b) Schematic diagram of the device wiring indicating separate control of the quantum point contact gate voltages V_{q1} , V_{q2} , and V_{q3} and of the side gate voltages V_{g1} , V_{g2} , and V_{g3} .

V_{g2} , which were varied in a raster pattern. We repeated this measurement for a series of interdot tunnel conductances ranging from $G_{\text{int}} \approx 0$ to $G_{\text{int}} \approx e^2/h$ to determine how interdot electron tunneling affects coupled dot interactions in the strong field regime. In this communication we describe several such measurements, at filling factors $\nu=2, 3$, and 4.

Figures 2(a)–2(d) summarize the results of this measurement at $\nu=2$ ($B=7$ T). Each panel is an inverted grayscale image of the logarithm of the measured double dot conductance versus V_{g1} on the horizontal axis and V_{g2} on the vertical axis; dark spots indicate high conductance, and bright areas indicate low conductance. The panels are arranged in order of increasing interdot tunnel conductance G_{int} , measured separately.³⁰ In Fig. 2(a) ($G_{\text{int}} \approx 0.01 e^2/h$), current flows at an array of points; the points are split in pairs along the diagonal $V_{\text{av}} = (V_{g1} + V_{g2})/2$ direction, corresponding to adding charge to both dots. The array of points of current flow is the signature of small interdot tunnel conductance: because the numbers of electrons N_1 and N_2 on the two dots are quantized, current only flows at the points where the Coulomb blockade is lifted simultaneously for both dots. As G_{int} is increased in subsequent panels, the splitting between

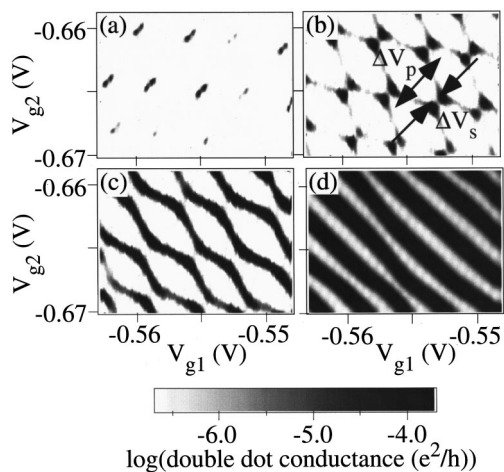


FIG. 2. Inverted grayscale images of the logarithm of the measured double dot conductance at $\nu=2$ plotted vs side gate voltages V_{g1} on the horizontal axis and V_{g2} on the vertical axis. Dark spots indicate high conductance, and bright areas indicate low conductance. The panels are arranged in order of increasing interdot tunnel conductance G_{int} , with $G_{\text{int}} =$ (a) 0.01, (b) 0.21, (c) 0.68, and (d) $0.96 e^2/h$.

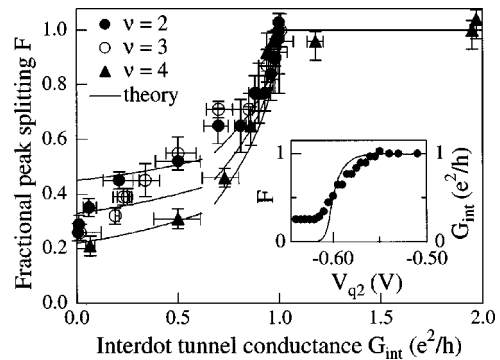


FIG. 3. Measured fractional peak splitting F plotted vs interdot tunnel conductance G_{int} , determined separately, for filling factors $\nu=2$ (closed circles), $\nu=3$ (open circles), and $\nu=4$ (closed triangles). The error bars indicate both scatter and systematic errors in calibration of the center point contact conductance. Also plotted are calculations of F from the theory of Golden and Halperin (Refs. 8–10). Matveev *et al.* found similar results (Refs. 11 and 12). The theory has been scaled to include a residual interaction energy at small $G_{\text{int}} \geq 0.2 e^2/h$. Three different scalings have been used to provide the best match to the three different filling factors, with $\nu=2$ at the top, $\nu=3$ in the middle, and $\nu=4$ at the lowest trace. Inset: Measured fractional peak splitting F (circles) and interdot tunnel conductance G_{int} (line) plotted vs center point contact gate voltage V_{q2} for $\nu=2$. F saturates strongly at a finite value as interdot conductance G_{int} goes to zero.

points of conductance in the V_{av} direction increases, and lines of conductance grow out from these points along the curves that separate charge configurations with different values of the total number of electrons $N_{\text{tot}} = N_1 + N_2$. By Fig. 2(d) ($G_{\text{int}} \approx 0.96 e^2/h$), current flows along an array of essentially straight lines separating regions with different lowest energy values of N_{tot} . This evolution is qualitatively similar to that observed in previous experiments in zero magnetic field.¹ As in the zero field case, the topological change from an array of points to an array of lines indicates that the transition from completely separate dots to completely joined dots is complete.

One pronounced difference between the strong field case described here and the zero field case¹ is that the transition from well separated to completely joined dots is complete when there is one quantum (e^2/h) of interdot tunnel conductance, in contrast to two quanta ($2e^2/h$) for the zero field case. This indicates that frustrated charge configurations of the double dot are relaxed when just the outer edge states in the two dots have merged. A second important difference is that in a strong magnetic field, we observe a larger finite peak splitting for small interdot conductance ($G_{\text{int}} \ll e^2/h$). This splitting indicates a large residual interaction energy relative to the charging energy that is not due to interdot tunneling interactions. This residual splitting is discussed below.

We quantify the transition from separate to joined dots by measuring the fractional peak splitting F , which is proportional to the amount by which interdot interactions lower the energy of the system. The fractional peak splitting is $F \equiv 2\Delta V_s / \Delta V_p$, twice the ratio of the peak separation ΔV_s in the diagonal V_{av} direction of the charging diagram to the periodicity of the array ΔV_p . Figure 3 is a plot of the fractional splitting F versus the interdot tunnel conductance G_{int} , measured separately, for three different filling factors:

$\nu=2$ (closed circles), 3 (circles), and 4 (closed). The $\nu=2$ values were measured from the data set represented in Fig. 2. The results for $\nu=4$ ($B=3.1$ T) were measured on the same device and at the same cooldown; those for $\nu=3$ ($B=4.8$ T) were measured on the same device during a different cooldown. Also plotted are theoretical results for the fractional peak splitting (lines) calculated by Golden *et al.*⁸⁻¹⁰ for the case of one conducting channel for the low and high interdot tunnel conductance limits. Matveev *et al.* found similar results.^{11,12} The theoretical calculations have been scaled to account for an additional interaction energy seen for $\nu=2$ (top), 3, and 4.¹⁰ The scaling was chosen to match the F vs G_{int} data for $G_{\text{int}} > 0.2e^2/h$, as discussed below.

For all three filling factors, the transition from well separated to completely joined dots is complete ($F=1$) when the interdot tunnel conductance $G_{\text{int}} = e^2/h$. This is in agreement with the theories of Golden *et al.*⁸⁻¹⁰ and Matveev *et al.*^{11,12} for the case of one channel of interdot tunnel conductance. For the $\nu=2$ and 3 cases, it is not feasible to increase the interdot tunnel conductance to $G_{\text{int}} > e^2/h$ because of cross capacitance and the need to maintain 2DEG depletion beneath the point contact gates. We do obtain data for $G_{\text{int}} \cong 2e^2/h$ for $\nu=4$ as shown. The charging diagram and fractional peak splitting remain saturated at their $G_{\text{int}} \cong e^2/h$ behavior as the interdot tunnel conductance increases to two edge channels in the constriction, in agreement with theory.

In the range between $G_{\text{int}} \cong (0.2-1)e^2/h$, we find good agreement between the measured fractional splitting and theory, as shown in Fig. 3, if we use an enhanced dot interaction energy that increases with magnetic field. The shape of the F vs G_{int} curve for $G_{\text{int}} > 0.2e^2/h$ is similar for all three filling factors. At very low interdot conductance $G_{\text{int}} < 0.2e^2/h$, the observed fractional peak splitting rolls off to a lower, but still finite, value. The inset of Fig. 3 plots both the measured splitting F (circles) and the measured interdot conductance G_{int} (line) versus the center point contact gate voltage V_{q2} for filling factor $\nu=2$. The saturation of splitting at low interdot conductance is evident.

It is reasonable that the fractional splitting is modified in strong magnetic fields, because the electrostatics of quantum dots are strongly modified. In zero magnetic field, the fractional peak splitting at $G_{\text{int}}=0$ is $F=C_{\text{int}}/C_{\Sigma}$ where C_{int} is the interdot capacitance, and C_{Σ} is the total dot capacitance.^{1,3,9,10} In the strong field regime the electrons in each dot form concentric metallic rings (the edge states) separated by insulators (the incompressible regions).^{27,28} The capacitance of a ring is less than the capacitance of a disk of the same diameter. In addition the capacitance between the outer rings on the two dots is more sensitive to the interdot separation than is the capacitance between two disks. These simple considerations can qualitatively explain much of the weak tunneling regime of Fig. 3. A quantitative model should include the full internal electrostatics of each dot as well as dynamical effects.

The authors thank P. Brouwer and B. I. Halperin for helpful discussions and comments on the manuscript and R.

G. Beck, D. Bozovic, L. Chen, D. Davidovic, M. Drndic, S. Pohlen, and M. A. Topinka for experimental assistance. Supported at Harvard was provided by NSF Grant No. DMR-98-02242, ONR Grant No. N00014-99-1-0347, and the MRSEC program of the NSF under Award No. DMR-98-09363; support at the University of California at Santa Barbara was provided by Grant AFOSR No. F49620-94-1-0158 and by QUEST. One of the authors (D. S. D.) acknowledges support by the DOD NDSEG fellowship program.

- ¹C. Livermore, C. H. Crouch, R. M. Westervelt, K. L. Campman, and A. C. Gossard, *Science* **274**, 1332 (1996).
- ²F. R. Waugh, M. J. Berry, D. J. Mar, R. M. Westervelt, K. L. Campman, and A. C. Gossard, *Phys. Rev. Lett.* **75**, 705 (1995).
- ³C. H. Crouch, C. Livermore, R. M. Westervelt, K. L. Campman, and A. C. Gossard, *Appl. Phys. Lett.* **71**, 817 (1997).
- ⁴N. C. van der Vaart, S. F. Godijn, Y. V. Nazarov, C. J. P. M. Harmans, J. E. Mooij, L. W. Molenkamp, and C. T. Foxon, *Phys. Rev. Lett.* **74**, 4702 (1995).
- ⁵A. S. Adourian, C. Livermore, R. M. Westervelt, K. L. Campman, and A. C. Gossard, *Superlattices Microstruct.* **20**, 411 (1996).
- ⁶R. H. Blick, R. J. Haug, J. Weis, D. Pfannkuche, K. v. Klitzing, and K. Eberl, *Phys. Rev. B* **53**, 7899 (1996).
- ⁷L. W. Molenkamp, K. Flensberg, and M. Kemerink, *Phys. Rev. Lett.* **75**, 4282 (1995).
- ⁸J. M. Golden and B. I. Halperin, *Phys. Rev. B* **53**, 3893 (1996).
- ⁹J. M. Golden and B. I. Halperin, *Phys. Rev. B* **54**, 16757 (1996).
- ¹⁰J. M. Golden, Ph.D. thesis, Harvard University, 1997.
- ¹¹K. A. Matveev, L. I. Glazman, and H. U. Baranger, *Phys. Rev. B* **53**, 1034 (1996).
- ¹²K. A. Matveev, L. I. Glazman, and H. U. Baranger, *Phys. Rev. B* **54**, 5637 (1996).
- ¹³G. Klimeck, G. Chen, and S. Datta, *Phys. Rev. B* **50**, 2316 (1994).
- ¹⁴C. A. Stafford and S. Das Sarma, *Phys. Rev. Lett.* **72**, 3590 (1994).
- ¹⁵P. L. McEuen, E. B. Foxman, U. Meirav, M. A. Kastner, Y. Meir, N. S. Wingreen, and S. J. Wind, *Phys. Rev. Lett.* **66**, 1926 (1991).
- ¹⁶P. L. McEuen, E. B. Foxman, J. M. Kinaret, U. Meirav, M. A. Kastner, N. S. Wingreen, and S. J. Wind, *Phys. Rev. B* **45**, 11419 (1992).
- ¹⁷R. C. Ashoori, H. L. Stormer, J. S. Weiner, L. N. Pfeiffer, S. J. Pearton, K. W. Baldwin, and K. W. West, *Phys. Rev. Lett.* **68**, 3088 (1992).
- ¹⁸P. L. McEuen, N. S. Wingreen, E. B. Foxman, J. Kinaret, U. Meirav, M. A. Kastner, Y. Meir, and S. J. Wind, *Physica B* **189**, 70 (1993).
- ¹⁹R. C. Ashoori, H. L. Stormer, J. S. Weiner, L. N. Pfeiffer, K. W. Baldwin, and K. W. West, *Phys. Rev. Lett.* **71**, 613 (1993).
- ²⁰N. C. van der Vaart, M. P. de Ruyter van Steveninck, L. P. Kouwenhoven, A. T. Johnson, Y. V. Nazarov, C. J. P. M. Harmans, and C. T. Foxon, *Phys. Rev. Lett.* **73**, 320 (1994).
- ²¹O. Klein, C. de C. Chamon, D. Tang, D. M. Abusch-Magder, U. Meirav, X.-G. Wen, M. A. Kastner, and S. J. Wind, *Phys. Rev. Lett.* **74**, 785 (1995).
- ²²O. Klein, D. Goldhaber-Gordon, C. de C. Chamon, and M. A. Kastner, *Phys. Rev. B* **53**, R4221 (1996).
- ²³N. B. Zhitenev, R. C. Ashoori, L. N. Pfeiffer, and K. W. West, *Phys. Rev. Lett.* **79**, 2308 (1997).
- ²⁴N. C. van der Vaart, L. P. Kouwenhoven, M. P. de Ruyter van Steveninck, Y. V. Nazarov, C. J. P. M. Harmans, and C. T. Foxon, *Phys. Rev. B* **55**, 9746 (1997).
- ²⁵B. W. Alphenaar, A. A. M. Staring, H. van Houten, M. A. A. Mabesoone, O. J. A. Buyk, and C. T. Foxon, *Phys. Rev. B* **46**, 7236 (1992).
- ²⁶B. W. Alphenaar, A. A. M. Staring, H. van Houten, I. K. Marmorosk, C. W. J. Beenakker, and C. T. Foxon, *Physica B* **189**, 80 (1993).
- ²⁷J. M. Kinaret and N. S. Wingreen, *Phys. Rev. B* **48**, 11113 (1993).
- ²⁸D. B. Chklovskii, *Phys. Rev. B* **47**, 12605 (1993).
- ²⁹B. I. Halperin, *Phys. Rev. Lett.* **60**, 1542 (1982).
- ³⁰The conductance of the center point contact G_{q2} is measured versus point contact gate voltage V_{q2} with the side gates energized to experimental conditions and the outer point contacts energized just to depletion. G_{int} is obtained by adding an additional calibrated lateral shift to account for the effect of bringing the outer point contact gates into the tunneling regime.